Experimental Data Collection and Modeling for Nominal and Fault Conditions on Electro-Mechanical Actuators

Edward Balaban[1], Abhinav Saxena[2], Kai Goebel[3], Carl S. Byington[4], Matthew Watson[5], Sudarshan Bharadwaj[6], and Matthew Smith[7]

[1] *NASA Ames Research Center, Intelligent Systems Division, MS 269-3, Moffett Field, CA 94035, USA*
edward.balaban@nasa.gov
[2] *SGT Inc., NASA Ames Research Center, Intelligent Systems Division, MS 269-4, Moffett Field, CA 94035, USA*
abhinav.saxena@nasa.gov
[3] *NASA Ames Research Center, Intelligent Systems Division, MS 269-4, Moffett Field, CA 94035, USA*
kai.goebel@nasa.gov
[4,5,6,7] *Impact Technologies, LLC, 2029 Cato Avenue, State College, PA, 16801, USA*
carl.byington@impact-tek.com
matthew.watson@impact-tek.com
sudarshan.bharadwaj@impact-tek.com
matthew.smith@impact-tek.com

ABSTRACT

Being relatively new to the field, electromechanical actuators in aerospace applications lack the knowledge base compared to ones accumulated for the other actuator types, especially when it comes to fault detection and characterization. Lack of health monitoring data from fielded systems and prohibitive costs of carrying out real flight tests push for the need of building system models and designing affordable but realistic experimental setups. This paper presents our approach to accomplish a comprehensive test environment equipped with fault injection and data collection capabilities. Efforts also include development of multiple models for EMA operations, both in nominal and fault conditions that can be used along with measurement data to generate effective diagnostic and prognostic estimates. A detailed description has been provided about how various failure modes are inserted in the test environment and corresponding data is collected to verify the physics based models under these failure modes that have been developed in parallel. A design of experiment study has been included to outline the details of experimental data collection. Furthermore, some ideas about how experimental results can be extended to real flight environments through actual flight tests and using real flight data have been presented. Finally, the roadmap leading from this effort towards developing successful prognostic algorithms for electromechanical actuators is discussed.*

1 INTRODUCTION

Electro-mechanical actuators (EMA) are presently used in numerous aerospace applications, from robotic applications to thrust vector control of rocket engines, where they accomplish a range of rotational and translational functions. There is an increasing tendency, however, to move towards all-electric aircraft and spacecraft designs (i.e., without any hydraulic systems), which promises an even wider use of EMAs in the future (Blanding, 1997, Jensen et al, 2000). With actuators being some of the more safety-critical components of an aerospace system, an undetected actuator failure can lead to serious consequences – as has happened on multiple occasions in the past (for instance, Alaska Airlines MD-83 Flight 261, horizontal stabilizer actuator failed due to insufficient lubrication and excessive wear of its jack screw (NTSB Report, 2000)). Even though actuators have been studied extensively from a functional point of view – in order to help develop new and improved designs – studies from a health management point of view have been rather limited due to unavailability of operational fault

data from fielded applications and lack of experimental studies with seeded fault tests due to high risks and costs involved. EMAs in aerospace systems work in highly noisy environments, i.e. must be studied thoroughly to characterize their inherent modalities that may then be later isolated in real noisy environments for effective diagnostics and prognostics with reduced uncertainty (Byington et al, 2004-1, Byington et al, 2004-2). This calls for a systematic effort towards understanding the EMAs and their behavior under various fault conditions through affordable but realistic experiments.

This paper describes our efforts towards carrying out a systematic, affordable, and realistic study through extensive experiments for EMA health management that faces several challenges. These experiments have been designed keeping various factors in mind as mentioned next briefly. EMAs are composed of electrical, electronic, and mechanical subsystems integrated together, which results in additional intricate failure modes and effects. Based on extensive Failure Modes, Effects and Criticality Analysis (FMECA) studies, literature review, and accessible industry experience, critical fault modes have been identified and incorporated through provisions for corresponding seeded fault tests. These faults in various sub-assemblies need to be successfully and efficiently detected, identified, and isolated using only a limited set of sensor signals available. Furthermore, sensor failures pose a grave challenge and therefore sensor failure identification and isolation must be accomplished through the test environment as well [6]. Since actuators are often under-instrumented, physics-based modeling of failure modes and mechanisms can help make the most of the available measurements to accomplish effective diagnostics and prognostics in real-time [5, 7]. Therefore, this effort also includes developing various physics based models at different levels of granularity covering a wide variety of critical failure modes. These models must be validated and verified, which will be accomplished through data collected from the experimental setup. EMAs being quite complex assemblies, a systematic study is needed to carry out controlled experiments to understand and isolate the effects of various factors. Therefore a design of experiments was included in the study. Last but not the least, experimental studies must be connected and correlated to real flight experiments, hence two identical test setups have been accomplished of which one employs real full size test article intended for use in lab experiments whereas the other small scale test rig is conducive for actual flight tests. For experiments under realistic scenarios use of load profiles from actual flights has been planned.

Of the various kinds of actuators, EMAs were chosen for this study because of their growing role in the aerospace field. They are relatively compact and can offer high power-to-weight ratios and motion velocities. We also decided to concentrate on actuators suitable for use with flight control surfaces, to build on the previous F-18 flight experiments at NASA Dryden Flight Research Center (Jensen et al, 2000), which led us to the choice of linear, ballscrew type EMAs.

The rest of the paper is organized as follows: first the design of our baseline experiments is discussed, from the equipment used to the test parameters (Section 2). Next the nominal models of actuator behavior, mechanical and thermal, are covered along with the results of their validation using test stand data (Section 3). Section 4 describes our techniques for fault injection and some of the fault models we will be utilizing are described in Section 5. Finally, our future plans are outlined and conclusions for this phase of our work are presented.

2 DESIGN OF EXPERIMENTS

In order to reach valid and objective conclusions from an experimental study experiments should be carefully designed to facilitate a statistically meaningful analysis. Design of Experiments (DoE) is a methodical approach to plan such a set of experiments. The three basic principles of DOE, i.e. replication, randomization and blocking, are intended to improve the design and effectiveness of diagnostic and prognostic algorithms. First, a thorough FMECA study is carried out to identify dominant failure modes before the testing phase, followed by listing dominant operating modes, system state variables (control variables and internal variables), and external factors along with noise and crosstalk. All these variables are then classified into control variables (inputs), nuisance variables (noise), and response variables (outputs). These variables are then quantized into a respective range of feasible values. The DOE must minimize the influence of these nuisance variables on the experimental data.

From the PHM perspective first a baseline set of data is collected to characterize healthy system. Next, data are collected while varying the degree of fault in the system to simulate fault progression. The goal of DOE here becomes to collect data from a test setup, which is reliable, unbiased and covers all dominant operating modes and fault modes so that the designed algorithms detect and predict with a high degree of confidence while the number of experiments performed remains practically tractable. If the number of Control variables is large for a particular operating mode, one may choose to start with a two-level full factorial design which yields a first-order model and helps weed out any insignificant factors. The number of experiments determines the statistical soundness and level of precision obtained from data collected. In

practice, to reduce the affects of system and measurement noise, the concepts of replication and repetition are employed in order to meet the necessary tolerances. Similarly, any memory effects can be affectively handled by randomizing the control variables. Both repetition and replication lead to an increase in the number of experiments. However, they also improve the confidence in the gathered data.

Since the number of system variables is large in the EMA experiments, a carefully designed DoE is considered. The details regarding various chosen response and control variables are discussed next.

2.1 EMA Test Stand

An Electro-mechanical actuator (EMA) test stand has been designed and built in collaboration between Impact Technologies and NASA Ames Research Center (Figure 1) (Balaban et al, 2009, Smith et al, 2009, Swerdon et al, 2009). It is being used in experiments studying diagnostic and prognostic methods for ball-screw jams, spalling, abnormal wear, backlash, as well as electronics and power failures. Dynamic load for the test actuator is provided by a powerful Moog 886 load EMA, capable of producing up to 5 metric tons of opposing force. The control system of the stand allows custom load profiles and long-term, endurance testing and data recording. The instrumentation suit includes a load cell, accelerometers, high-precision position sensors, and temperature sensors. The data acquisition system allows recording of data samples with frequency of up to 64 kHz.

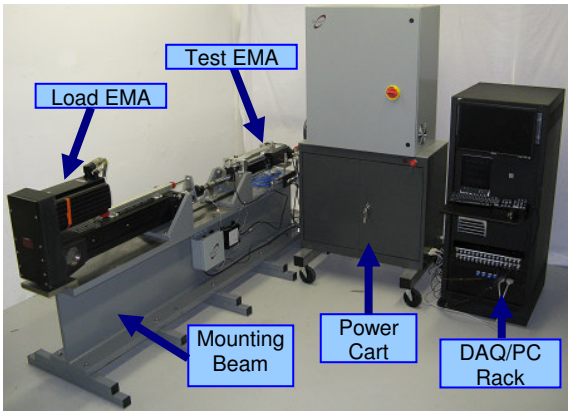

Figure 1: NASA's EMA test stand

In addition, Impact's Dynamic ElectroMechanical Actuator (DEMA) test bed (Figure 2) is also being used for initial model validation. The DEMA test platform consists of a small (1000 lbf) EMA that is loaded by a pneumatic cylinder. The system features two independent controllers, a Proportional Air electronic pressure regulator (EPR) and a Galil motor controller, whose behavior is corralled by a third, custom software-based controller hosted on a PXI controller. This sub-scale test platform was used to allow model development and validation in parallel with construction of the test stand described above.

Figure 2: Impact's Dynamic ElectroMechanical Actuator (DEMA) test stand

2.2 Baseline EMA Characterization

In designing the baseline experiments, our goals were two-fold: first one to validate our nominal EMA models and the second to provide a comparison basis for the fault-injected tests. The design of experiments principles described above were used to come up with a comprehensive, yet realistic set of motion profile types, load levels, and other experiment conditions (realistic in the sense of being able to execute all of the experiments in a reasonable amount of time). Our rationale for selecting experiment parameters is presented in the subsequent section.

2.3 Motion Profiles

Rectangular (step): this profile simulates rapid changes in actuator position. While likely not encountered in most applications, this profile allows evaluating the response time and profile following characteristics of an actuator.

Trapezoidal: Related to the rectangular profile, a trapezoidal profile incorporates a more gradual position change and is mainly intended to the test the steady state error characteristics of the actuator.

Sinusoidal: a sinusoidal profile is a good approximation for many instances of motion performed by actuators in real-life applications, which usually involve a period of gradual acceleration in the beginning and gradual deceleration at the end (for instance: normal aileron deflection, flap deployment, landing gear retraction and deployment). Also included in the tests are sinusoid sweep profiles, where the period of the sine wave gradually decreases throughout the test run.

Triangular: triangular profile, with the most drastic changes in velocity and acceleration, is well suited for detection of backlash (described further in the paper),

where such abrupt changes expose abnormalities in motor current and vibration levels consistent with that fault.

The amplitude of motion used was 50 and 100 mm (with step profiles also done at 0 mm). Linear velocity varied from 6 cm/s to 12 m/s. Duration of each run was 30 seconds, except for sine sweep profiles, where the motion lasted 120 seconds.

2.4 Load Profiles

The load profiles were executed in both tensile and compressive direction. The following load levels were used: 0 lbs, 500 N, 4500 N, 8500 N. The highest load was just under the maximum continuous rated load for the test actuators (8750 N).

3 NOMINAL MODEL

3.1 Mechanical Actuator Model

The Impact team has created a dynamic model of an electromechanical actuator system in the Simulink® environment of the MATLAB. This model can be used to represent the physics of degradation and its effects on the performance of components, systems or subsystems within the overall actuator system. The developed EMA Simulink® model is shown in Figure 3, while the schematic of an EMA is shown in Figure 4.

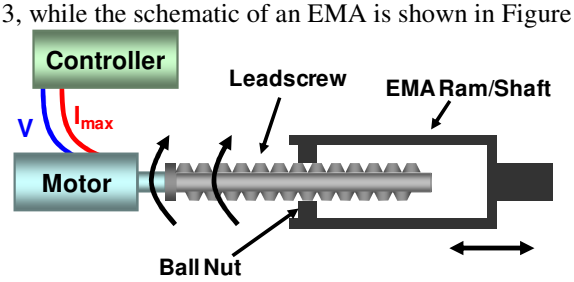

Figure 4: Schematic of an electromechanical actuator

The model incorporates blocks for the various components within the EMA, such as the brushless DC motor, leadscrew and ball nut, ram, and output shaft. It also contains blocks for components such as the gearbox and encoder, which can be selected or deselected by the user, since these components may not be present on all EMAs. Similarly, the user may also select the type of control for the EMA, with the available choices being position control, velocity control, or torque control.

The assumptions made in creating this EMA model are listed below**:**

1) Brushless DC motor drives leadscrew
2) Motor modeled as L-R circuit
3) Leadscrew, ball-nut, and ram modeled as rigid components with mechanical efficiencies
4) Shaft angular acceleration proportional to excess torque (motor torque, less damping and load torques)

$$V = RI + L\frac{dI}{dt}$$

$$\tau = k_t I$$

$$\tau = J\ddot{\theta} + B\dot{\theta} + \tau_l$$

where I is the motor current, V is the motor voltage, R is the winding resistance, L is the winding inductance, τ is the motor torque, kt is the torque constant of the motor, J is the rotor inertia, B is the damping on the rotor, and τl is the load torque acting on the rotor shaft. A virtual test bed environment was also developed in Simulink® to allow simulation of the developed model, critical faults, and other external effects (i.e., loads, control inputs, etc) that contribute to prediction uncertainty, as well as to collect actuator response data from virtual sensors embedded in the virtual test bed.

Simulations performed by the authors initially

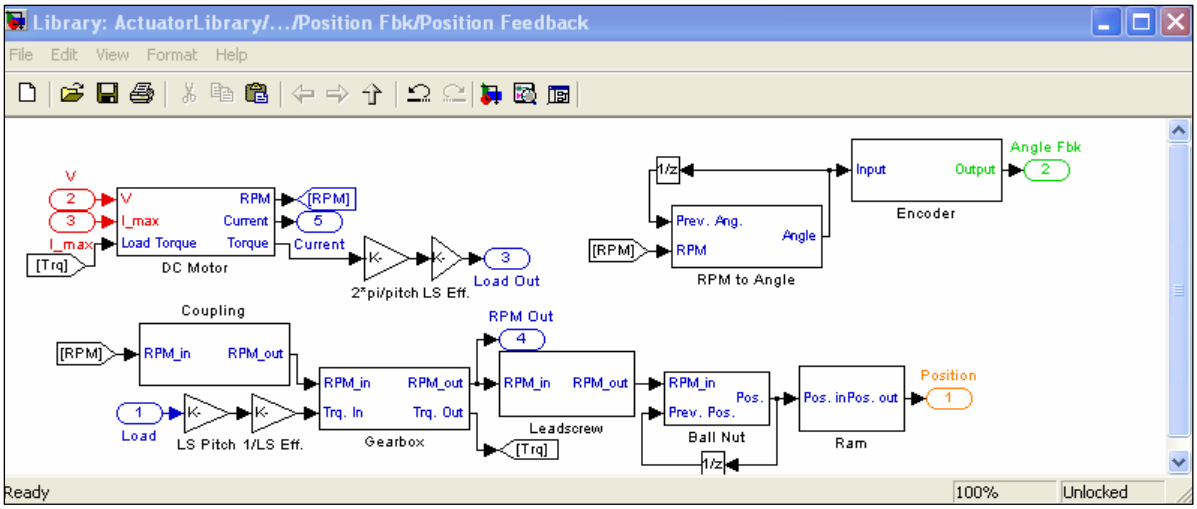

Figure 3: Dynamic model of an electro-mechanical actuator

consisted of observation of the system response to various position and load profiles under expected healthy conditions. For instance, Figure 5 shows the response of the EMA to a sinusoidal position profile with a step change in the load. As seen, the controller and drive are able to maintain the specified position profile (top left plot) against the jump in the load. The bottom left plot shows a step change in the current drawn corresponding to the change in the load (top right plot). The bottom right plot shows the temperature of the EMA motor windings and surface. As expected, the higher current draw from t=20 seconds causes a faster rise in both temperatures.

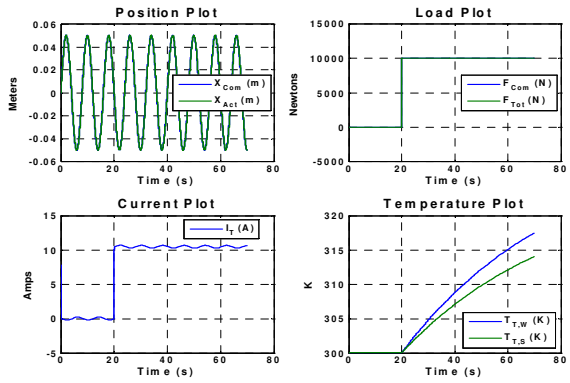

Figure 5: EMA model response to sine position and step load profiles

A similar second-order dynamic model of an EMA for Matlab and Simulink was created at NASA Ames and verified for the Moog MaxForce 883-023 actuator using experimental data provided by the Moog Corporation. The goal was to verify the modeling parameters, performance of the sensor suit, and repeatability of results after disassembly/reassembly of test actuators. The latter was needed to ensure that when a fault was injected into an actuator component (disassembly and reassembly were required for the set of faults injected subsequently), the rest of the components were not inadvertently affected. Four runs were executed, with actuator disassembled and reassembled between each run. Two load types were used: spring and opposing force. The loads had a low setting (860 lb for spring, 900 lb for opposing force) and a high setting (1725 lb for spring, 1800 for opposing force). Position of the test actuator rod was specified by two motion profiles: triangular and sinusoid. In all, data from 32 experiments was utilized – 8 from each run.

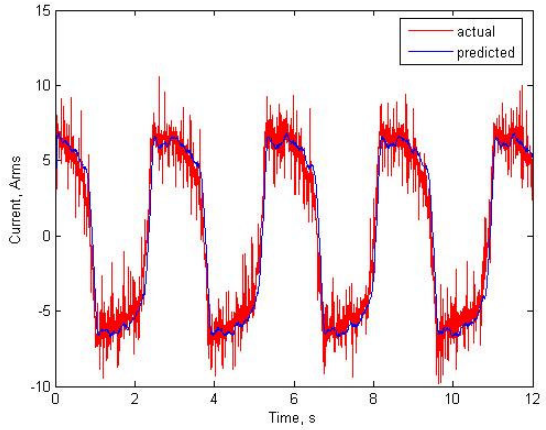

Figure 6: Run 3, sinusoid profile, opposing force 900 lb load

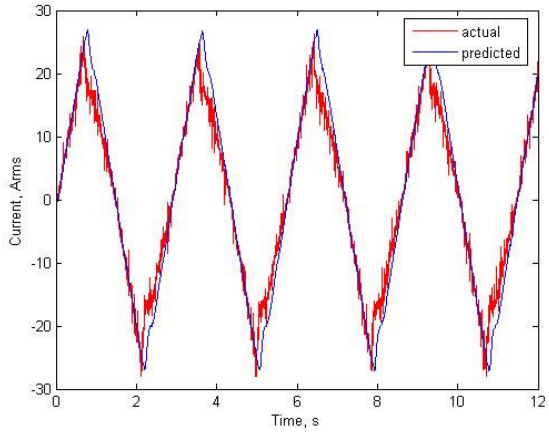

Figure 7: Run 5, triangular profile, spring force 1725 lb load**.**

The results demonstrated a close match of the model to actuator behavior on the test stand. The average error between predicted and measured current drawn by the motor was 7.12% (RMS), calculated across all of the experiments. The maximum error was 9.96%, the minimum – 5.82%.

3.2 Thermal Model

In addition to modeling the electrical and mechanical components of the EMA, a thermal model of the motor was also implemented. The thermal model provides an estimate of the temperature of the rotor windings and motor surface. The main source of heat is produced by the current in the windings. This heat generation can adversely affect the system during prolonged use or under higher loading conditions, during which the motor temperature rises rapidly due to the large current draw. Operating a motor at these high temperatures can have severe consequences, including the risk of burning

out the windings or demagnetization of the rotor permanent magnets. Winding shorts and stator rubs also lead to frictional heat generation.

The thermal model provides a method of estimating the motor temperature at various operating conditions. The thermal model of the EMA motor is described in Figure 8. As the figure shows, the model treats the motor windings as a lumped system, and determines their temperature at each time step, based on the input heat (I2R losses), and the heat lost to the surface of the motor. The motor surface in turn loses heat to the ambient through convection and radiation.

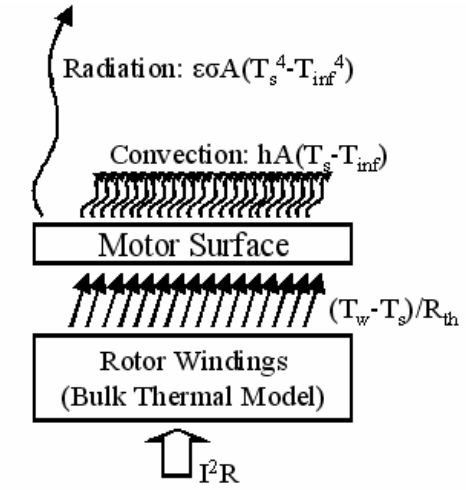

Figure 8: Thermal model of EMA

The equations that govern the thermal model simulation are given below.

$$\left(I^2R - \frac{T_{w,i-1} - T_s}{R_{th}}\right)dt = m_w C_{pw}(T_{w,i} - T_{w,i-1})$$
$$\frac{T_{w,i-1} - T_s}{R_{th}} = hA(T_s - T_{\inf}) + \varepsilon\sigma A(T_s^4 - T_{\inf}^4) \quad (1)$$

where:

I	:	Winding Current
R	:	Winding Resistance
Rth	:	Thermal Resistance
dt	:	Simulation Time Step
mw	:	Mass of Windings
Cpw	:	Specific Heat of Windings
h	:	Heat Transfer Coefficient
A	:	Motor Surface Area
σ	:	Stefan's Constant
ε	:	Surface Emissivity
Ts	:	Motor Surface Temperature
Tinf	:	Ambient Temperature
Tw,i-1	:	Winding Temperature at Timestep i-1
Tw,i	:	Winding Temperature at Timestep i

3.3 Thermal Model Validation

The thermal model of the actuator motor was initially validated with thermocouple data from the DEMA test rig. Figure 9 compares the model-estimated motor surface temperature with the motor thermocouple readings for one of the baseline runs on the DEMA rig. It is to be noted that the thermocouple readings have been averaged over 1 second intervals to minimize sensor noise. As seen, the thermal model does a good job of estimating the motor surface temperature over the full hour of baseline testing. The maximum error between the model estimate and the actual surface temperature is around 0.84 K (~1.5 F), while the RMS error is around 0.42 K (~0.8 F). Of special interest are the trends in the thermocouple readings, which the thermal model accurately predicts.

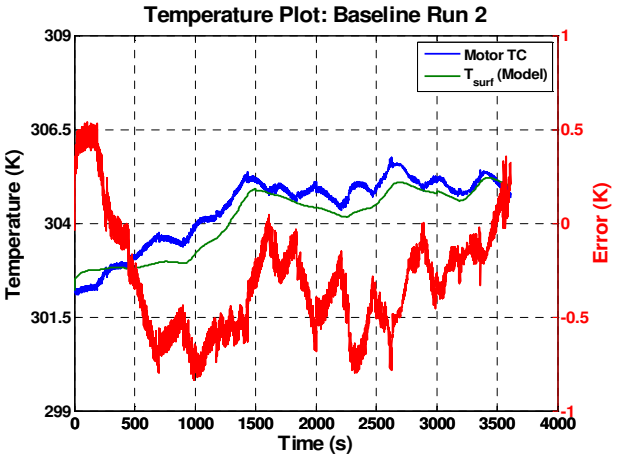

Figure 9: Validation of thermal model of actuator motor with test stand data

Figure 10 also shows the ball nut and ambient thermocouple readings (also averaged over 1 second intervals), as well as the model-estimated winding temperature. Due to physical and logistics issues on the setup, the winding temperature could not be measured. However, the model provides a method of estimating the winding temperature from the measured motor surface temperature.

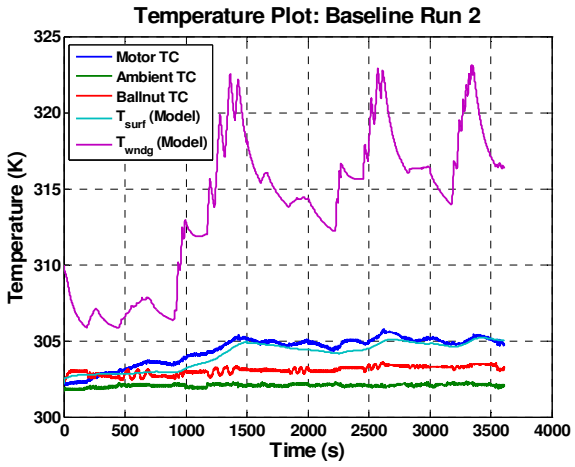

Figure 10: Winding and surface temperature prediction

4 FAULT INSERTION

The authors performed an analysis of the critical failure modes relevant to EMA systems. The criticality of the failure mode was determined from estimates of the frequency of occurrence (based in part on historical data), and the severity of fault. The severity assessment considered the effects on the operation of the EMA, the system-level effects (such those on an aircraft landing gear or weapons actuation system), and ultimately, the overall effects on aircraft performance. Based on this analysis, it was determined that backlash, return channel jam, winding shorts, rotor shaft eccentricity, insufficient lubrication, and control sensor faults are the most critical faults affecting EMA operation. Thus, it was decided to focus on these faults during the seeded fault testing on the EMA test rig. The following sections discuss the available options that were considered for seeding these faults.

4.1 Backlash

Backlash is simulated by mounting a specially-designed backlash adapter between the load cell and the test actuator. The adapter consists of a piston moving inside a cylinder and supported on the test actuator side by a threaded plug screwed into the cylinder.

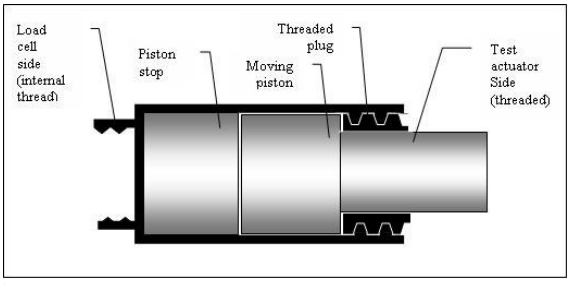

Figure 11: Backlash adapter

The amount of backlash is adjusted by rotating the plug in and out. Once the desired gap is established, the position of the plug is fixed with a set screw.

By adjusting the insertion depth of the threaded plug and the load during the tests, we created data sets with varying rates of backlash progression. Using this approach, backlash progression was simulated in significantly shorter periods of time than is possible by to achieve by normal use, where material of the actuator has to physically wear away.

It is also less intrusive than an alternative method of replacing bearing balls with smaller diameter ones. The latter method, while likely mimicking the physical manifestations of backlash with more fidelity, is expensive, time consuming, and introduces additional uncertainty because of the actuator disassembly and reassembly.

4.2 Return channel jam

Return channel is a component of a ballscrew actuator that transports balls in the circuits within the nut from the end of a circuit back to its beginning, as the nut travels along the rotating screw. A jam in the return channel, caused, for example, by a piece of debris or a deformed ball, would stop that circulation and could lead to catastrophic consequences. Return channel jams are of a particular interest to us because they are a class of faults that cannot easily be addressed by design modifications.

To reproduce a jam fault, a threaded cylindrical opening is machined through the nut collar and one of the return channels. A thin screw is then gradually inserted into the return channel, thus simulating the fault range from a partial channel obstruction to a fully developed jam.

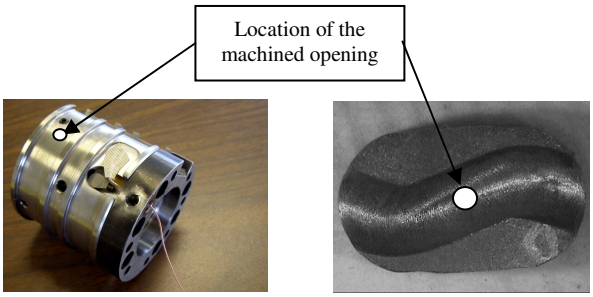

Figure 12: Ball return jam injection

4.3 Winding Shorts

Motor winding shorts occur when one or more turns within the winding coil get shorted together, thus creating a path for the current that bypasses the shorted turns. The most extreme case would be a complete

short of the winding. Partial winding shorts increase the current draw to the motor, owing to the lower winding resistance. This causes excess heating of the motor winding, as compared to baseline operation. Motor overheating leads to undesirable effects, such as demagnetization of the permanent magnets or winding burn-out. Overheating can also lead to insulation breakdown in the windings, which in turn further induces shorts. In addition, winding shorts also induce eccentricity in the rotor shaft orbit, due to uneven electromagnetic forces on the rotor. In extreme cases, eccentricity can lead to stator rub, causing further heating and damage to both the stator and the rotor. Winding shorts are thus extremely damaging to all classes of electric motors.

Comparison of Seeding Techniques

The authors conducted an analysis of various methods of seeding or simulating winding shorts in a brushless DC (BLDC) motor.A winding short would reduce the winding resistance, inductance, torque constant, and back EMF constant. The reduction in winding inductance mainly affects the transient current response of the winding to an applied voltage. Likewise, the torque constant, which affects the torque generated per unit current and represents the torque available to accelerate the shaft, affects the time taken to attain full speed (in the absence of load torques, and neglecting speed-dependent damping terms) and again is only relevant during transients. Similarly, the reduction in back EMF constant, which causes a higher current draw since the back EMF opposing the applied voltage is lower, is dependent on the speed of the system. However, a reduction in winding resistance would cause a higher current draw in all states of the system.

While physically shorting a winding is the most physically representative option, it would involve permanently damaging the motor and was thus not attractive for our testing. Instead, methods for simulating winding shorts were pursued. Winding shorts can be simulated by causing an increased current draw in other ways, among which is the addition of a resistance in parallel to the winding. As seen in the equations below, this resistance in parallel, however, would draw a current independent of the motor speed. The increased current draw would simply be V/R, where V is the applied voltage, and R is the resistance. Thus, this approach does not represent the speed dependency of the back EMF constant nor does it consider the effect on winding inductance and torque constant. Regardless, it is representative of the reduction in winding resistance and represents the fault well during steady state operation.

$$I_w = \frac{V_{applied} - V_{back}(RPM)}{R_w} = \frac{V_{excess}(RPM)}{R_w} \qquad I = \frac{V_{applied}}{R} \tag{2}$$

As such methods for simulating this fault by connecting a resistance in parallel with one of the windings in the motor were pursued.

Figure **13** below shows the first option, where the resister is in parallel with one phase and is grounded to the center tap of the windings. The figure shows the current drawn by the motor during three stages of the commutation cycle. As seen, during two stages of the commutation cycle (extreme left and extreme right sections of the figure), the drive would be supplying an additional current (above the baseline value) to one winding, whereas during the second stage of the commutation cycle (middle section in the figure), the winding currents to the other two windings would be the same as the baseline current.

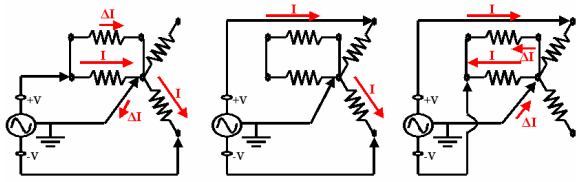

Figure 13: Seeding winding shorts using resistance in parallel with winding

Figure **14** shows the second option, which includes connecting the fault-seeding resistance between a winding leg and the source (drive) ground. This option also mimics the higher current draw associated with a winding short for the same two phases of the commutation cycle (assuming that the resistance was hooked to the same phase) as option 2. Thus, option 3 would be physically equivalent to option 2 in this respect.

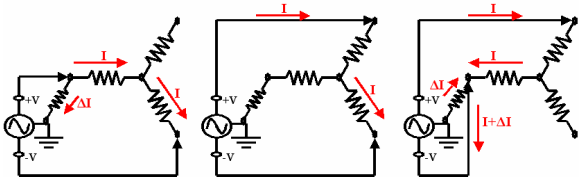

Figure 14: Seeding winding shorts using resistance between winding leg and ground

The final choice between these two options depends to a certain extent on the availability of a center tap

access point. Some wye-connected three phase BLDC motors provide access to the center tap of the phase windings, while others do not. In the case of delta-connected motors, there obviously isn't a center tap. If a center tap is available, option 1 is the preferred method. However, if there isn't a center tap, the grounding could be to the source ground (typically the ground on the motor drive – see option 2). In our case, center tap access was available on the motor in the EMA test rig, and the grounding was to the winding center tap (Option 1).

Winding Short: Quantitative Analysis

In order to determine the resistor values to use in this fault simulation, a quantitative analysis was conducted. Since the effect of this true winding shorts are speed dependent, it is difficult to quantify the value of this resistance from the point of view of the level of the winding short desired. An alternative approach would be to have this resistance draw a current that is some pre-determined fraction of the maximum current rating of the motor windings. In our work, the windings within the BLDC motor of interest each have a resistance of 0.9 Ω, and the current rating is 10 A. Connecting a 25 Ω resistance in parallel with one winding would cause the drive to supply an additional current to this new resistance. At a voltage level of 230 V (which is the maximum voltage supplied to the windings), this additional current would be ~10 A. This is comparable to the maximum winding current, and would thus be expected to seed an average fault level close to 50% winding short. The use of 25 Ω, 50 Ω, and 150 Ω resistances in appropriate combinations would allow the seeding of five levels (besides baseline), viz., 10%, 14.29%, 25%, 33.33%, and 50% (1/10th, 1/7th, 1/4th, 1/3rd, and 1/2) of winding short fault. These are the fault levels that were determined for the seeded fault testing on the actuator rig.

4.4 Rotor Shaft Eccentricity

Motor shaft eccentricity faults occur when the centerline of the rotor within the motor is displaced from the centerline of the stator. This would lead to an uneven air gap between the stator and the rotor, thus causing uneven electromagnetic forces on the rotor from the stator. Thus, the shaft orbit follows a complex pattern, which leads to undesirable forces on the motor bearings, in turn causing atypical vibration levels. In extreme cases, the motor air gap may reduce to zero, in which case the rotor would rub against the stator. This would lead to excessive frictional heating and potentially damaging vibration levels. The excess heating could also lead to winding insulation breakdown, thus inducing winding shorts, which in turn exacerbate the eccentricity of the shaft orbit, thus leading to a destructive cycle of escalating fault levels within the motor.

In the simplest cases, shaft eccentricity can be static or dynamic. Static eccentricity involves a rotor centerline displacement from the stator centerline, which is steady with time. With dynamic eccentricity, the rotor shaft displacement from the stator centerline wobbles with the rotor angular position. The difference between static and dynamic eccentricity is illustrated in Figure **15**.

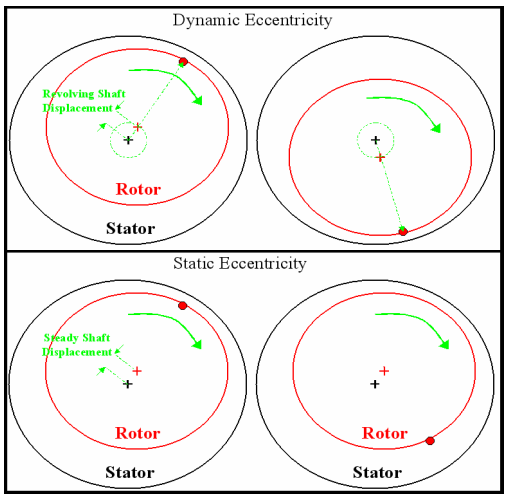

Figure 15: Difference Between Static & Dynamic Eccentricity

Static eccentricity may be seeded by displacing the rotor bearing using shims. It may be necessary to remove any sealing mechanism between the rotor bearing and the stator housing, such as o-rings, to create the necessary gap. Dynamic eccentricity is more complex, but may be induced by other means. Since one of the causes of dynamic eccentricity is an imbalance in the mass distribution of the shaft, dynamic eccentricity may be seeded in the motor by placing additional mass on one side of the rotor shaft. This is illustrated in the bottom picture in
Figure **15**.

The level of the dynamic eccentricity fault may be varied by changing the amount of the mass imbalance. This may be achieved by stacking weights on top of each other or next to each other on the rotor shaft. Several options exist for increasing the severity level of a dynamic eccentricity fault. Weights may be added in the tangential direction (Option 1), the radial direction (Option 2), or the axial direction (Option 3). Option 1 involves using segments of a semi-cylindrical weight. One disadvantage of this option is that the effects of the fault level are highly nonlinear. This is also a disadvantage with Option 2, since the excess unbalanced moment of inertia induced in the rotor shaft

varies not only with the mass added, but also with the square of the radial distance from the shaft center. Also, due to the limited space in the motor, this option would require the weights to be concentric, thin semi-cylindrical pieces, which would take significant machining effort. Option 3 was thus judged the best option, from the point of view of linearity of the fault level with increasing number of weights, and also the ease of implementation.

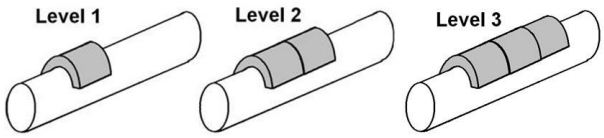

Figure 16: Dynamic Eccentricity Fault Simulation

Rotor Eccentricity: Quantitative Analysis

The brushless DC motor on the test setup has a shaft with a moment of inertia of 102 kg-cm^2. The motor shaft is 32 mm in diameter. About 50 mm of the shaft is free, and can be used to add excess unbalanced mass. A semi-cylindrical steel piece with an inner diameter of 32 mm and an outer diameter of 70 mm, with a length of 50 mm, would weigh (assuming a high density metal) around 3 kg. Using the relation for the moment of inertia of a hollow cylindrical mass:

$$J = \frac{m}{2}\left(r_2^2 - r_1^2\right) \qquad (3)$$

where J is the moment of inertia, r_2 and r_1 are the outer and inner radii, respectively, and m is the mass of the hollow cylinder, the excess moment of inertia of the semi-cylindrical segment (which wraps around 1/2 of the shaft) would be ~7.27 kg-cm^2. Thus, the excess unbalanced inertia would be about 7.13% of the rotor shaft inertia. If the load inertia were of the same order as the motor shaft inertia, the excess moment of inertia (with respect to the total of the motor shaft and the load inertias) would correspond to a fault level of roughly 3.65%. As Figure **16** indicates, a semi-cylindrical steel weight such as described above could be cut into axial segments, and segments could be added one at a time to the rotor shaft to seed increasing levels of fault severity, up to a maximum of about 3.65% dynamic eccentricity level.

4.5 Resolver Fault

BLDC motor controllers obtain position (or rotor angle) feedback from devices such as encoders or resolvers. In the NASA EMA test rig, this feedback comes from a resolver. This resolver is a critical component for the operation of the motor, since the controller commands the current to the motor based on the error between the position command and the resolver feedback. Thus, faults in the resolver would affect the ability of the motor to attain the commanded position. Resolvers consist of a shaft with a primary winding and two secondary windings (Brown et al, 2008). The primary winding is supplied with a time-varying voltage signal, which induces varying voltages in the secondary windings as the shaft rotates. If the secondary windings are spaced 90^o apart on the shaft, then one winding would put out a signal proportional to the sine of the shaft angle, while the other would put out a signal proportional to the cosine of the angle. Knowledge of the magnitudes and signs of the angle sine and cosine uniquely determines the shaft angle. If the resolver shaft were coupled to the motor shaft, then the resolver would indicate the motor shaft angle.

Encoders, on the other hand, consist of a light source with a rotating disk containing reflecting sectors. The disk would reflect light whenever a reflecting sector lined up with the light source (and/or transmit light when a transparent sector lined up with the source). A detector is used to count the number of pulses generated as the shaft rotates. If two rings with reflecting sectors were arranged in quadrature on the encoder disk, then the magnitude and direction of the shaft speed could be uniquely determined from the quadrature pulse counts per unit time.

Resolver faults may be seeded in several ways. Two ways considered in this work are shown in Figure **17**. As the figure shows, the first option is to interrupt the power supply to the resolver. This may be achieved by placing a relay in line with the resolver power line, and controlling the operation of the relay using a timing signal. Varying the duty cycle of the timing signal would allow control over the severity level of the fault.

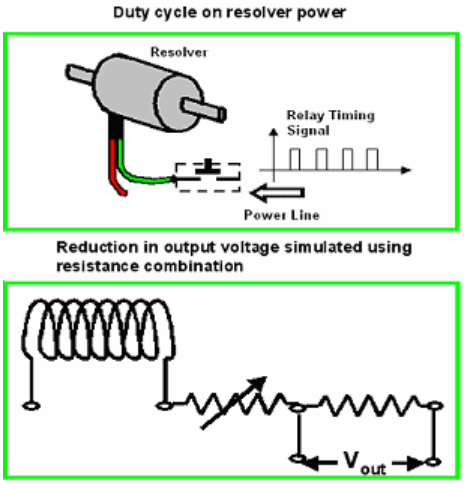

Figure 17: Resolver Fault Seeding Options

Physically, the varying duty cycle would simulate transient loss of power to the resolver. The motor controller would not receive resolver feedback during these intervals when the power was off, and would thus see a "non-rotating shaft." The controller would command the motor to run at full speed to match the position command. When the resolver power came back on, the controller would be able to tell the absolute shaft position (resolvers are absolute position measuring devices, as opposed to incremental encoders). Thus, the controller would try to move the shaft to the required position (based on the position command), but this might mean reversing the shaft rotation to compensate for the motion at maximum speed during the period when the resolver was off. The result would be an erratic back-and-forth motion of the motor shaft. Some controllers would shut down the motor when the resolver feedback was lost. If the controller was set up to automatically resume motion when the resolver feedback came back on, then the controller would try to follow the position command once more when the feedback was reestablished. This would also result in jerky motion of the motor shaft, but this would be a "stop and go" motion as opposed to the earlier back-and-forth motion of the shaft. In the case of encoders, this option for seeding faults would simulate damage to some of the encoder disk sectors, thus causing loss of electrical pulses in the feedback whenever a damaged sector lined up with the light source.

Another option for seeding a resolver fault involves simulating a channel mismatch. Electromechanical resolvers typically have two channels, which operate in quadrature mode to yield information on the speed of the shaft, as well as its direction of rotation. In a healthy resolver, both channels would put out time-varying voltages, whose amplitudes would be the same. However, with channel mismatches, one of the channel voltages would be reduced in amplitude, and this would falsify the shaft position information derived from the quadrature voltages. As the bottom half of
Figure **17** shows, the reduction in the voltage amplitude on one channel of the resolver output may be simulated by connecting a resistance combination in series with one of the windings, and the level of the fault may be varied by varying the value of one of the resistances. With encoders, this option might not be physically meaningful, unless the output voltage level of the encoder pulses were reduced to the point where the controller could no longer read the pulses. In effect, the pulse voltage level would drop below the threshold where the controller could identify the pulses. Other fault seeding options also exist for resolvers, such as inducing (or simulating) a resolver winding short similar to the motor winding short described above. In the current work, the resolver fault was simulated by varying the duty cycle of the resolver power.

5 FAULT MODELING

5.1 Dynamic Eccentricity

The dynamic EMA model described in Section 3.1 also includes fault blocks within the various components. Using these blocks, faults can be modeled as gain, bias, and/or noise on various parameters and signals. For example, Figure 18 shows the simulation of a dynamic eccentricity motor fault. This fault is simulated by specifying a bias on the motor shaft centerline position. This bias rotates with the shaft angle, and thus the eccentricity of the motor shaft with respect to the stator centerline is "dynamic." The fault level simulated was 10% dynamic eccentricity, i.e., the rotor centerline was displaced from the stator centerline by 10% of the motor air gap. The top left plot of the figure shows the EMA response to a sinusoidal position profile with a steady loading (top right plot) under the influence of this fault. As seen, the system is able to follow the position command, despite the fault. This occurs because the motor controller is able to compensate for the fault by changing the current draw. This may be seen in the lower plots of the figure. The lower right plot shows a small part of the lower left phase 1 current plot. From the bottom right plot, it is seen that the current drawn by the motor phase is different from the baseline current.

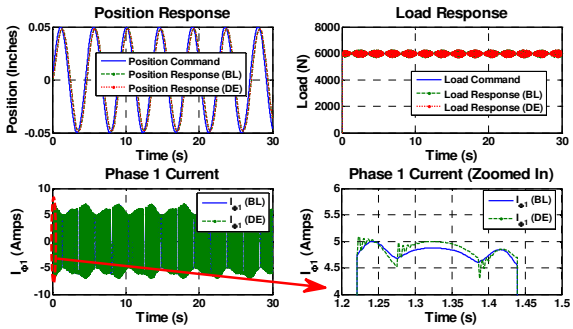

Figure 18: Simulation of a dynamic eccentricity motor fault

5.2 Winding Shorts

Similarly, a winding short was simulated in the motor (Figure 19). This was achieved by using a gain block to reduce the "number of winding turns" parameter on just one phase (phase 1). The fault level simulated was 20%, i.e., a gain of 0.8 was placed on the number of winding turns parameter, effectively bypassing 20% of the phase winding. The top left plot of the figure shows

the system response to a sinusoidal position profile and steady load profile (top right plot). As the bottom left plot in the right half of the figure shows, the winding short causes a rise in the motor current, which compensates for the reduced torque constant (owing to the reduced effective number of windings). Thus, the actuator is still able to follow the specified position profile (top left plot in the figure). The increased current draw may be seen more clearly in the bottom right plot, which zooms in on a segment of the current plot to the bottom left.

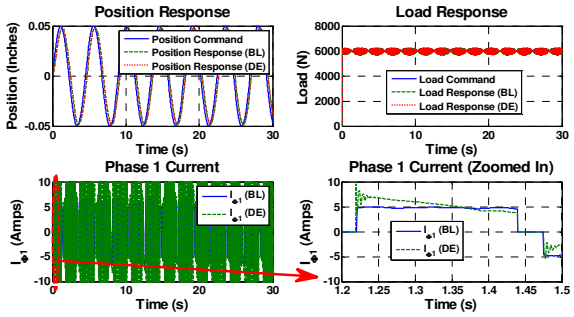

Figure 19: Simulation of a winding short

5.3 Ballscrew Jam

The decreased efficiency of the ballscrew due to a jam of the return channel in one of the circuits was also modeled using Matlab. An assumption was made that the either the channel is clear or it is completely blocked. A partial obstruction causing a slow down of ball movement is theoretically possible, but considered to be unlikely.

The model was verified using experimental data from Moog Corporation. Both spring and constant load types were used with the following load levels: 0, 860/900 lbs and 1725/1800 lbs. Sinusoid and triangular motion profiles were executed. The results showed a good correlation between theoretical predictions and experimental results. The average error between predicted and measured current drawn by the motor was 8.34% (RMS), calculated across all of the experiments. The maximum error was 9.88%, the minimum – 5.60%. Some of the results are illustrated on Figure 20 and Figure 21.

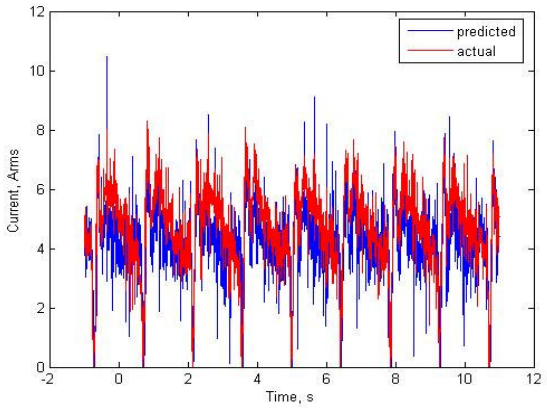

Figure 20: Sinusoid motion profile, 900 lbs opposing Force

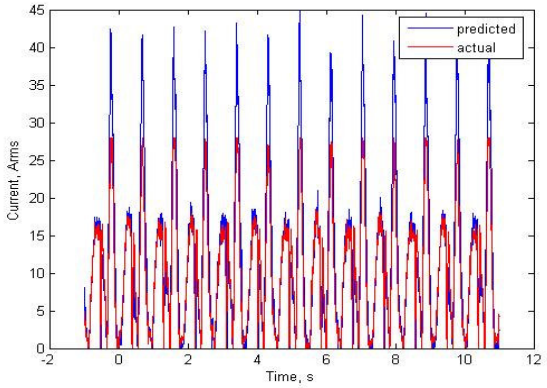

Figure 21: Triangular motion profile, 1725 lbs spring force load

6 FUTURE WORK

6.1 Other Faults to be Injected

Spalling: the term spalling referes to development of indentations in metal surfaces at high stress contact points. A severe case of a spall may result in metal flakes separating from the surface, creating potentially dangerous debris. In the case of a ball screw, where the contact surfaces of the nut and the screw (as well as the balls) may be subject to spalling, one of the consequences may be increased vibration, which can lead to damage of other actuator components. The likelihood of an EMA developing a spall in one of its components over its lifetime is not insignificant. Spalling will be injected by machining a small "seed" imperfection onto the surface of the screw and then monitoring its development as the actuator is excercised through the various motion regimes.

Insufficient lubrication: The lubricant in the EMA will be gradually depleted, by disassembling the actuator at regular intervals and removing some of the lubricant each time. A series of experiments with

contaminated lubricant is also being planned, where increasing amounts of metal debris are introduced into it (to simulate the side effects of spalling and normal wear).

6.2 Active Diagnosis and Prognosis

To build on our investigation of on the suitable set and parameters of motion and load profiles, we would also like to pursue research into active diagnosis and prognosis of EMAs.

Just as pilots take the essential control surfaces on an aircraft through their range of motion before take-off and gauge whether the range is nominal and the motion is unfettered, a PHM system with an active element could execute motion profiles during ground checkout targeted towards identifying a specific set of critical faults and analyze sensor output. This could be especially beneficial if the desired profiles are not usually encountered during the normal flight operations (such as triangular profiles). Such a system could automatically adjust the remaining set or the parameters of profiles being executed based on the analysis of the preceding ones (e.g. if a fault needs to be confirmed or disambiguated, or if its severity needs to be established).

6.3 Development of Flyable Data Collection Test Stand

While it is possible to simulate some of the desired environmental conditions in ground experiments, testing our equipment and methods in presence of vibrations, noise, G-loads, and temperature variations inherent to flight will be invaluable. It is also desirable to ensure that our data acquisition, processing and prognostic health management algorithms satisfy real-time performance requirements.

The main idea for the experiments is to fly a scaled-down EMA test stand (Figure 20) that contains two test actuators – one nominal and one injected with a fault, and one load actuator. The stand is currently being developed in collaboration between NASA Ames Research Center and California Polytechnic Institute. The load can be switched during flight from the healthy to the faulty actuator, thus collecting both baseline and off-nominal data under the same conditions. The rod position of the test actuators and the load applied to them will be scaled down from the corresponding values for one of the aircraft's control surfaces. The real-time data for the actuator position will come from the aircraft data bus. Load will be calculated from the using airspeed, altitude, air density, angle of attack, and other parameters, also obtained from the aircraft bus.

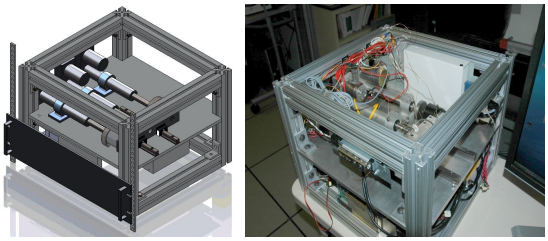

Figure 22: Portable EMA test stand

The sensor data collected on the stand will be directed into a prognostic health management system that will monitor performance of the test actuators for faults and, if a fault is detected, predict the effects on actuator performance and the remaining useful life. In addition, the data will be used to design motion and load profiles that are representative of flight conditions - to be used on the full-scale EMA test stands at NASA Ames and Impact Technologies.

6.4 Planned Flight Experiments

There are several efforts currently under way to both collect data on aircraft aimed on data collection on existing (hydraulic, in most cases) actuators and the aforementioned portable actuator test stand. The data from the standard actuators will be used to extract realistic load and motion profiles (to be used on the full-size EMA test stand at NASA Ames) and to better characterize the relevant flight environment. The test stand is currently being prepared to be flown on a UH-60 Blackhawk helicopter; other aircraft being considered for future experiments include C-17, F-18, S-3, and unmanned aerial vehicles.

7 CONCLUSION

This work described in the paper represents the first phase of joint EMA data collection and analysis activity at NASA Ames and Impact Technologies. During it equipment for collecting a variety of performance information (both in laboratory and flight conditions) has been constructed and experimental methodologies designed.

The team developed models to describe mechanical and thermal behavior of the actuators, which so far show a good match with experimental results. The models will be improved upon further, both to increase their accuracy and to incorporate component faults.

The methodology for injecting faults into the test actuators (backlash, ball screw jam, motor winding shorts, motor shaft dynamic eccentricity, and encoder faults) is described as well. The work on implementing them is currently under way.

Finally, plans for future work are outlined, including other fault modes considered for injection,

upcoming flight experiments, and ideas for algorithm development.

ACKNOWLEDGMENT

The authors would like to express their gratitude to colleagues at the Prognostic Center of Excellence (NASA Ames Research Center), Impact Technologies, NASA Dryden Flight Research Center, California Polytechnic State University, Georgia Institute of Technology, and Northrop Grumman Corporation for their extensive assistance with this research and preparation of the manuscript. They would also like to thank Paul Stoelting, Joel Rack and Simon Curran at Moog Corporation for their help in designing experiments, obtaining equipment, analyzing fault modes, and producing data used in this project.

The funding for the project was provided by the NASA Integrated Vehicle Health Management (IVHM) project under the Aviation Safety Program of the Aeronautics Research Mission Directorate (ARMD).

REFERENCES

(Blanding, 1997) D. E. Blanding, "An Assessment of Developing Dual Use Electric Actuation Technologies for Military Aircraft and Commercial Application," in IECEC Energy Conversion Engineering Conference, 1997.

(Jensen et al, 2000) S. C. Jensen, G. D. Jenney, and D. Dawson, "Flight Test Experience with an Electromechanical Actuator on the F-18 Systems Research Aircraft," in IEEE Digital Avionics Systems Conference, 2000.

(NTSB Report, 2000) "Loss of Control and Impact with Pacific Ocean Alaska Airlines Flight 26 McDonnell Douglas MD-83," *NTSB Report*, AAR-02/01, 2000.

(Byington et al, 2004-1) C. Byington, M. Watson, and D. Edwards, "Data-Driven Neural Network Methodology to Remaining Life Predictions for Aircraft Actuator Components," in IEEE Aerospace Conference, Big Sky, MT, 2004, pp. 3581-3589.

(Byington et al, 2004-2) C. S. Byington, M. Watson, D. Edwards *et al.*, "A Model-Based Approach to Prognostics and Health Management for Flight Control Actuators," in IEEE Aerospace Conference, Big Sky, MT, 2004, pp. 3551-3562.

(Moseler et al, 1999) O. Moseler, D. Juricic, A. Rakar *et al.*, "Model-based fault diagnosis of an actuator system driven by the brushless DC motor," in American Control Conference, 1999, pp. 3779-3783.

(Balaban et al, 2009) E. Balaban, A. Saxena, P. Bansal *et al.*, "A Diagnostics Approach for Electro-Mechanical Actuators," in IEEE Aerospace Conference, Big Sky MT, 2009.

(Smith et al, 2009) M. J. Smith, S. P. Bharadwaj, G. M. Swerdon *et al.*, "Experimental and Analytical Development of Health Management for Electro-Mechanical Actuators," in IEEE Aerospace Conference, Big Sky, MT, 2009.

(Swerdon et al, 2009) G. Swerdon, M. Watson, S. Bharadwaj *et al.*, "A Systems Engineering Approach to Electro-Mechanical Actuator Diagnostic and Prognostic Development," in Machinery Failure Prevention Technology (MFPT) Conference, 2009.

(Brown et al, 2008) D. W. Brown, D. L. Edwards, G. Georgoulas *et al.*, "Real-Time Fault Detection and Accommodation for COTS Resolver Position Sensors," in 1st International Conference on Prognostics and Health Management (PHM08), Denver, CO, 2008.

Edward Balaban is a researcher in the Diagnosis and System Health group at NASA Ames Research Center. His main areas of interest are diagnostics and prognostics of physical systems. He is currently the lead for actuator prognostics with the Diagnostics & Prognostics Group in the Intelligent Systems Division. During his years at Ames he participated in research and development of diagnostic and other autonomy elements for the X-34 experimental reusable launch vehicle, International Space Station, robotic astronaut assistants, autonomous planetary drills, and the future generation of autonomous micro-spacecraft. He received the Bachelor degree in Computer Science from The George Washington University in 1996 and the Master degree in Electrical Engineering from Cornell University in 1997.

Abhinav Saxena is a Staff Scientist with Research Institute for Advanced Computer Science at the Prognostics Center of Excellence, NASA Ames Research Center. His research focus lies in developing prognostic algorithms for engineering systems. He is a PhD in Electrical and Computer Engineering from Georgia Institute of Technology, Atlanta. He earned his B.Tech in 2001 from Indian Institute of Technology (IIT) Delhi, and Masters Degree in 2003 from Georgia Tech. Abhinav has been a GM manufacturing scholar and also a member of Eta Kappa Nu and Gamma Beta Phi engineering honor societies along with IEEE and ASME.

Kai Goebel received the degree of Diplom-Ingenieur from the Technische Universität München, Germany in 1990. He received the M.S. and Ph.D. from the University of California at Berkeley in 1993 and 1996, respectively. Dr. Goebel is a senior scientist at NASA Ames Research Center where he leads the Diagnostics

& Prognostics groups in the Intelligent Systems division. In addition, he directs the Prognostics Center of Excellence and he is the Associate Principal Investigator for Prognostics for NASA's Integrated Vehicle Health Management Program. He worked at General Electric's Corporate Research Center in Niskayuna, NY from 1997 to 2006 as a senior research scientist. He has carried out applied research in the areas of artificial intelligence, soft computing, and information fusion. His research interest lies in advancing these techniques for real time monitoring, diagnostics, and prognostics. He holds ten patents and has published more than 100 papers in the area of systems health management.

Carl S. Byington is a Professional Engineer and the Director of Systems Engineering at Impact Technologies and possesses over 17 years in the design, analysis and testing experience with mechanical, thermal, and fluid power systems. He currently performs as the Principal Investigator on the development of innovative prognostics and health management technologies for military and commercial customers, and he has successfully led numerous programs for the Army, Navy, Air Force, DARPA, and military OEMs. Prior to joining Impact, Carl worked at NASA Langley Research Center performing air breathing propulsion research, and more recently, the Penn State Applied Research Laboratory (PSU ARL) as the Department Head in Condition-Based Maintenance. Carl is a lead and co-author on 2 patents related to PHM technology, and he has published over 65 papers, book chapters, magazine and journal articles related to signal processing, data fusion, statistical analysis, model-based prognostics, and predictive health management.

Matthew J. Watson is a Manager of Dynamic Systems at Impact Technologies with 8 years experience in the design, development, and testing of diagnostic and prognostic systems. He has participated in the design of advanced feature development, fault classifcation, and dynamic systems modeling techniques for a variety of applications, including gas turbine, flight control, power transmission, drive train, electrochemical, fluid, and hydraulic systems. Prior to joining Impact, Matt worked in the Condition-Based Maintenance Department of PSU-ARL, where he focused on model-based PHM development of electrochemical and fuel systems. He has co-authored 23 papers related to advanced sensing techniques, signal processing, diagnostics and control, model-based prognostics, data fusion, and machinery health management and is co-author on 2 patents.

Sudarshan Bharadwaj received his undergraduate degree in Mechanical Engineering from the Indian Institute of Technology, Madras (India), as well as Masters and Ph.D. degrees in M.E. from the Pennsylvania State University. He has published several papers in his field. He has been involved with a number of projects at Impact related to the health management of gas turbine engines, aircraft, and ship systems, and has considerable experience in developing diagnostics and prognostics routines for these systems.

Matthew Smith is a Senior Project Engineer at Impact Technologies. During his tenure with Impact, Matthew has performed multiple efforts pertaining to actuator health management, diagnostic and prognostic system development, and experimental study of faulted system response and fault progression. Previously, as a research assistant at Penn State and the NASA Glenn Research Center, Matthew performed experimental and analytical oil-free bearing analyses. Matthew received his B.S. and M.S. degrees in Mechanical Engineering from The Pennsylvania State University. His research interests include: prognostic health assessment for bearing and actuator systems, grease degradation modeling, and fault classifier development.